Spatially compressed dual-wavelength excitation Raman spectrometer

John B. Cooper,[1,*] Sarah Marshall,[1] Richard Jones,[1]
Mohamed Abdelkader,[2] and Kent L. Wise[3]

[1]Department of Chemistry and Biochemistry, Old Dominion University, Norfolk, Virginia 23529, USA

[2]Intel Inc., 2501 NW 229th Street, RA3, Hillsboro, Oregon 97124, USA

[3]SGS North America, 8701 New Trials Drive, The Woodlands, Texas 77381, USA

*Corresponding author: jcooper@odu.edu

Received 7 March 2014; revised 9 April 2014; accepted 19 April 2014;
posted 23 April 2014 (Doc. ID 207883); published 20 May 2014

The design and operation of a novel dual-laser excitation Raman instrument is described. The use of two lasers of differing wavelengths allows for a Raman spectrum covering all fundamental modes of vibration to be collected while minimizing fluorescence and allowing for spatial compression of the spectrum on an imaging detector. The use of diode lasers with integrated distributed Bragg reflector gratings facilitates the use of an integrated thermoelectric cooler to allow collection of shifted excitation spectra for both of the lasers, further enhancing the rejection of fluorescence. An example is given, which uses seven excitation wavelengths for each laser to reconstruct the Raman spectrum of a solvent in the presence of a highly fluorescent dye by using a sequentially shifted excitation Raman reconstruction algorithm.

OCIS codes: (300.6450) Spectroscopy, Raman; (120.4570) Optical design of instruments; (300.2530) Fluorescence, laser-induced.

http://dx.doi.org/10.1364/AO.53.003333

1. Introduction

Raman spectroscopy provides a method to generate a vibrational spectrum of molecules and polyatomic ions. The vibrational spectrum, which is generated, is often used to identify the sample, a unique chemical or unique mixture of chemicals, much as a fingerprint is used to identify a person [1]. In order to generate a Raman spectrum, the chemical of interest is irradiated with a monochromatic excitation source. The use of a monochromatic source provides spectral resolution in the generated Raman spectrum, since use of a broadband source would result in the generation of broad peaks in the vibrational spectrum. Additionally, when photons from the excitation source impinge the chemical sample of interest, the majority of photons are scattered elastically, resulting in Rayleigh scattering of light, which is of the same wavelength as the excitation source. For this reason, the excitation source must be very intense in order to generate a detectable Raman signal. The requirement for an excitation source, which is intense and monochromatic, has resulted in the almost exclusive use of lasers as the excitation source in conventional Raman spectrometers.

Another consideration in the generation of Raman spectra is the wavelength of the laser. Since the efficiency of Raman scattering is inversely proportional to the laser wavelength raised to the fourth power, it is easier to generate a detectable signal using a laser with a short wavelength. However, a shorter wavelength corresponds to a larger amount of energy per photon, and this can result in the generation of fluorescence due to the population of excited

1559-128X/14/153333-08$15.00/0

electronic states within the sample or within impurities contained in the sample. Fluorescence generation is typically many orders of magnitude more efficient than Raman scattering. For this reason, the use of a short wavelength laser often results in a spectrum having a fluorescence signal much larger than the Raman signal, which prevents the Raman signal from being accurately measured [2]. Thus there are advantages and disadvantages for any laser wavelength that might be selected. This has resulted in several commercial instruments, which contain multiple excitation lasers, so that the user can select a laser wavelength appropriate for the particular measurement being made.

An additional consideration in choosing a laser is that the detector used to detect the Raman signal must be sensitive to the Raman photons being generated. Traditionally, the most popular detectors have been based on charge-coupled devices (CCD) [3]. The main advantages of CCDs as detectors in Raman spectroscopy are that they provide the possibility of obtaining a spectrum with a high signal-to-noise ratio due to the low readout noise and due to the multiplex advantage obtained by dispersing the photons spatially across one dimension of the CCD. Although it is desirable to use a long wavelength laser to avoid fluorescence, the quantum efficiency of a near-IR enhanced back-illuminated CCD approaches zero at wavelengths greater than 1100 nm. This presents a dilemma since the fundamental hydrogen-stretching vibrations occur at absolute energies of 2700–3300 cm^{-1} [4]. For these vibrations to be observed with a CCD detector, the excitation laser must be less than 807 nm. For this reason, one of the most common lasers used is a 785 nm laser [5,6]. Unfortunately, a 785 nm laser often results in the generation of significant fluorescence. Thus it is desirable to use a longer wavelength laser in order to reduce fluorescence. This, however, would result in the loss of important vibrational information about the chemical sample due to the loss of hydrogen stretching. The problem is often even worse than this because less-expensive front-illuminated CCDs cannot efficiently detect photons with wavelengths above 1060 nm. These less-expensive CCDs are often the detector of choice in handheld Raman instruments, and their use prevents excitation greater than 785 nm.

A solution to this problem has been to use longer wavelength lasers in combination with detectors, which are sensitive to longer wavelength photons. One example is the FT-Raman spectrometer, which typically uses a 1064 nm laser and a single element detector based on germanium or indium gallium arsenide in combination with an interferometer [7]. Although this solves the problem of detecting the entire Raman spectrum, including the hydrogen-stretching region, it creates new problems. One problem with FT-Raman is that the laser wavelength is so long, high optical power must be used to generate a sufficient Raman signal, which can result in sample burning. This problem is compounded by the fact that germanium (Ge) detectors and indium gallium arsenide (InGaAs) detectors are not shot-noise limited. Their poor performance relative to a CCD detector results in a lower-quality spectrum or the requirement of a much longer acquisition time, or even liquid nitrogen cooling of the detector in the case of Ge detectors.

A second solution has been to use InGaAs array detectors (which provide a multiplex advantage similar to a CCD) in combination with a long wavelength 1064 nm laser [8]. This method also has the problem of possible sample burning. In addition, even with the benefit of the multiplex effect, InGaAs array detectors are still much noisier than CCD detectors due to high readout noise, thus give a poorer quality signal-to-noise ratio. This is compounded by a fixed-pattern noise due to the nonuniformity of the individual InGaAs pixels. To a lesser extent, CCDs also suffer from pixel nonuniformity. However, unlike InGaAs arrays, which have only a single pixel in the vertical dimension (orthogonal to the wavelength axis), a CCD has multiple pixels in the vertical direction that are typically 25 μm or less in height. Vertical binning of CCD pixels alleviates any pixel nonuniformity.

In addition to the problem of fluorescence, there is also the consideration of spectral resolution. Since, the Raman signal is dispersed spatially across the CCD as a function of wavelength, spectral resolution can be limited by the size of the CCD detector (e.g., higher dispersion requires a larger format CCD for the same spectral range). In order to observe both the fingerprint region and the hydrogen-stretching region at higher dispersion, a large CCD detector must be used, adding expense and optical design considerations.

To address these issues, we present an optical design in which two lasers of different wavelengths are used as excitation sources to generate two Raman spectral regions on the same CCD in a spatially compressed format, which can be subsequently processed to generate a complete vibrational spectrum of the sample.

2. Instrument Design

A diagram of the spectrometer layout is shown in Fig. 1 along with the optical paths of both the excitation laser and the generated Raman signal. A custom designed dual 785/852 nm laser source in a TOSA package is used as the excitation source (Photodigm custom-PH785/852DBR080/100TB). As shown by the dashed line in Fig. 1, laser light from the excitation source is collimated by a lens (Thorlabs C230TME-B) and is then filtered by a custom dual-bandpass dielectric filter (Chroma z785/853x_v2), which only passes two narrow bands of light centered at the laser wavelengths (Fig. 2). These pass-bands are designed to pass the two wavelengths of the excitation lasers while rejecting emission outside of the pass-bands. After being filtered,

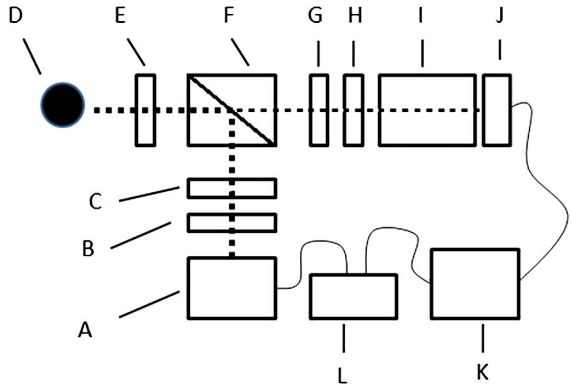

Fig. 1. Diagram of the Dual Laser Raman Instrument, showing the optical path from dual excitation laser (A), collimated by a lens (B), filtered by a dual notch filter (C), reflected by a dichroic-beamsplitter (F), and focused onto sample (D) by lens (E). Raman generated at sample (D) is collimated by lens (E), passed through the dichroic-beamsplitter (F), filtered by a long pass filter (G), and focused by lens (H) onto the slit of the spectrograph (I), where the Raman is detected by a CCD (J). A microcontroller (K) controls both the CCD (J) and a laser diode driver/temperature controller (L).

the light from the excitation source is reflected by a custom dichroic-beam splitter (Chroma z7t870lpxr_v1) designed to reflect light below 870 nm and to transmit light at longer wavelengths. The reflected light is focused by a lens (Thorlabs c240tme-B) onto a sample where it generates a Raman signal. The Raman signal is collected and collimated by the same lens and is passed through the dichroic beam splitter and then subsequently filtered by a long-pass filter (Chroma HQ865LP) with an O.D. > 5 at wavelengths less than 865 nm. The filter removes both excitation sources while passing the Stokes components of the Raman signal. After being filtered, the Raman signal is focused by a lens (Thorlabs 12.7 mm near-IR achromat, $F = 30$, AC127-30-B) onto the slit (Thorlabs 40 micron slit, s40r) of a custom spectrograph. The light in the spectrograph is collimated with a lens (Thorlabs 12.7 mm near-IR achromat, $F = 30$, AC127-30-B),

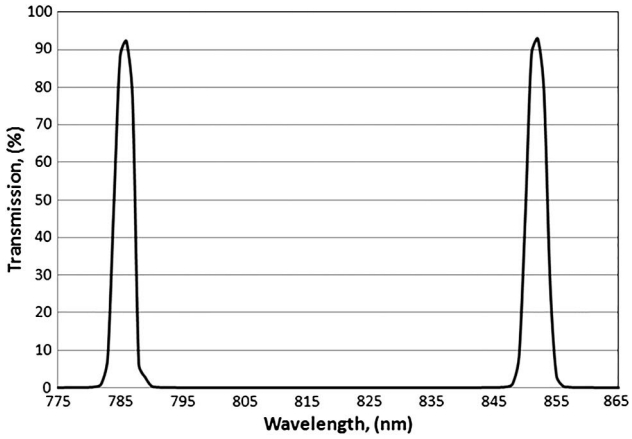

Fig. 2. Transmission spectrum of the dual-notch filter used to pass the 785 and 852 nm excitation lines of the dual laser.

and the collimated light is dispersed using a transmission volume holographic grating (Wasatch Photonics 1500 lpmm at 942.8 nm, SN1983). The dispersed Raman signal is focused with a lens (Thorlabs 25.3 mm near-IR achromat, $F = 45$, AC254-45-B) onto a back-thinned NIR-enhanced CCD detector (Hamamatsu S11500-1007). A custom dual-laser diode driver board with two integrated thermoelectric controllers (TEC) is electrically connected to the excitation source. The TEC design is based on the LTC1923 controller chip (Linear Technology), and the diode driver design is based on FDS9934C dual N/P field effect transistors (Fairchild). One of the TECs is used to control the temperature of the excitation sources. The second TEC is used to hold the temperature of the CCD at 15°C. A custom microcontroller board is used to programmatically control the CCD, the TECs, and the laser diode drivers. The board uses an MCORE MMC2114 (Freescale) for programmatic control and a Spartan XC2S50 FPGA (Xilinx) to drive the CCD readout electronics. The FPGA is programmed in VHDL using Foundation software, and the MCORE is programmed in C and assembly using the GNU compiler for MCORE. The size of the instrument including electronics is $5 \times 3 \times 1$ in. The small size is in keeping with the recent push for miniaturization of Raman instrumentation [9]. The instrument is connected via USB on the microcontroller board (FTDI FT245R) to an external computer running a Labview (National Instruments) data acquisition program. All software was written in house.

3. Detailed Description of the Excitation Source

Greater detail of the excitation source is given in Fig. 3. As shown, the excitation source consists of a dual-laser package on an aluminum nitride (AlN)

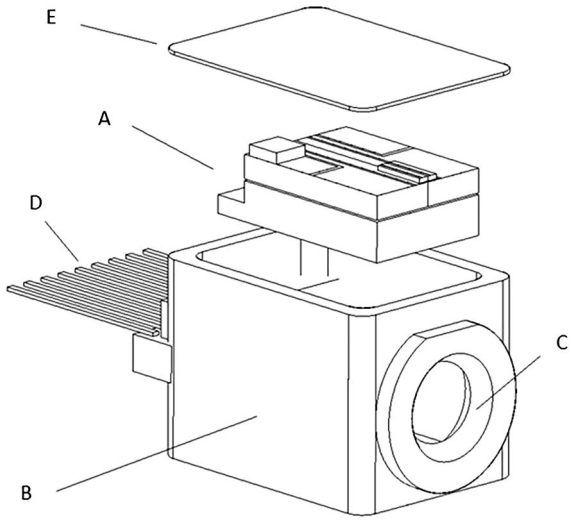

Fig. 3. Excitation source consists of a dual laser package mounted on an aluminum nitride (AlN) micro-bench (A) soldered inside of a TOSA electronic package (B) which has a windowed exit aperture (C), electrical feed-throughs (D), and a hermetical sealed lid (E).

microbench, which is placed inside of a TOSA electronic package (Kyocera), which has electrical feedthroughs and a windowed exit aperture to allow the laser light to pass out of the package. The total volume of this package is less than 1 cm^3. The dual-laser package is soldered (Au/Sn) to the inside base of the TOSA package to provide thermal contact and mechanical stability. A lid is used to hermetically seal the package. The electrical feedthroughs are used to electrically connect the device to the laser diode driver/temperature controller. Greater detail of the dual-laser package is given in Fig. 4. As shown, a distributed Bragg reflector (DBR) diode laser is soldered (Au/Sn) to a gold pad on the surface of a submount, which is made of AlN. The DBR laser is designed to emit ~852 nm laser light at 25°C. A gold pad on the surface of the DBR laser is electrically connected using gold wires to a second gold pad on the submount surface. A surface-mount thermistor is gold-wire bonded to a third gold pad on the surface of the submount. The surface of the thermistor is electrically connected to a fourth gold pad on the surface of the submount. A second (DBR) diode laser is soldered (Au/Sn) to a gold pad on the surface of a second submount, which is made of AlN. The DBR laser is designed to emit ~785 nm laser light at 25°C. A gold pad on the surface of the DBR laser is electrically connected using gold wires to a second gold pad on the submount surface. The two submounts are connected to the surface of a thermoelectric cooler using conductive epoxy. The separation between the emitting cavity faces of the two lasers is approximately 400 μm. Both lasers are driven at 200 mA (5 V) providing an optical output power of ~70 mW. The small mass of the subassembly allows for rapid temperature tuning of the lasers with minimal current draw. For example, the temperature of the lasers can be tuned ±5°C to a new temperature in ~200 ms with a temperature stability of 0.01°C and a maximum current draw of 50 mA at 3 V. This is valid up to a maximum ΔT from laser ambient of 30°C. The ambient temperature of the lasers using an adequate passive heat sink is ~32°C.

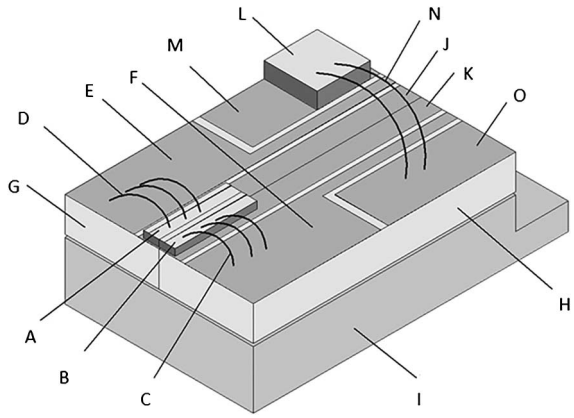

Fig. 4. Detailed schematic of the AlN microbench is shown. Two DBR lasers (A, B) are soldered to isolated gold pads (J, K) and electrically connected to additional isolated gold pads (E, F) of opposite polarity via gold bond wires (C, D). A thermis is electrically connected via gold bond wires (N) to an additional isolated gold pad (O) of opposite polarity; all gold pads are bonded to an AlN microbench (H); the micro-bench (H) is soldered to a Peltier thermoelectric cooler (I); the DBR lasers (A, B) emit at 785 and 852 nm, respectively.

4. Description of the DBR Diode Laser

Greater detail of the DBR diode lasers is given in Fig. 5. As shown, a laser cavity is fabricated on the topside of the GaAs substrate. A Bragg grating is fabricated adjacent to the rear facet so that, at a given temperature, light of a specific wavelength is reflected back into the laser cavity. The laser light emits from the end of the laser cavity, which opposes the Bragg grating. In Fig. 1, the orientation of the excitation source is such that the two images generated by the two lasers at the sample are projected to the slit of the spectrograph so that both images lie vertically on the slit. The separation between the images on the slit is approximately 400 μm.

5. Modes of Operation

Two modes of operation for the spectrometer are possible. In the serial mode of operation, only one laser is activated at a time and the spectrum from each laser is acquired in sequence by electronically shifting-out each horizontal row of pixels and vertically binning them together to form a spectrum. In the parallel mode of operation, both lasers are activated simultaneously, and both spectra are collected during the same integration period. Since the excitation sources are spatially separated, the resulting Raman spectra are offset along one dimension of the CCD. This spatial separation is depicted in Fig. 6, where the direction of offset is normal to the direction of dispersion on the CCD. In the parallel mode, vertical binning of the horizontal rows of pixels is performed separately for the two offset regions. The advantage of serial mode is the ability to independently set the integration time for each laser. This facilitates using the full dynamic range of the detector while avoiding saturation for both regions. Alternatively, the parallel mode

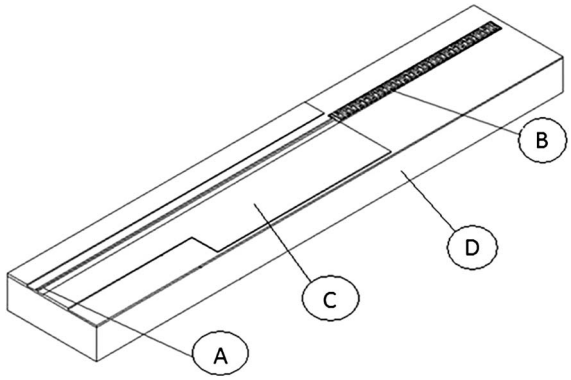

Fig. 5. Detailed schematic of a single DBR laser is shown with the emitting face of the diode cavity (A), reflective Bragg grating (B), gold pad electrodes (C), and AlN mount (D).

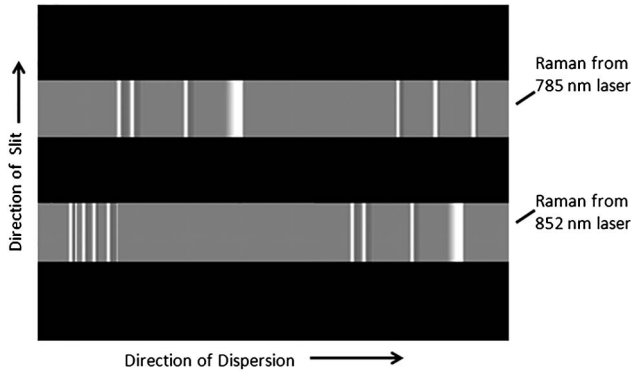

Fig. 6. Depiction of a CCD image is shown where dispersion of two different Raman spectra occurs on the x axis of the CCD and spatial separation of the spectra occurs on the y axis of the CCD. As shown, the top spectral image is generated by a laser having a shorter wavelength (e.g., 785 nm) than the laser generating the bottom spectral image (e.g., 852 nm).

of operation offers the advantage of minimizing spectral acquisition time.

6. Spectral Results and Processing

Figure 7 shows a plot depicting the two laser positions as well as the two Raman spectral regions generated by the two lasers for an acetaminophen standard. The two Raman spectral regions correspond to the spatial dispersion of the spectra onto the CCD, and both cover a range of approximately 1800 cm^{-1}. As shown, the spectra are plotted in absolute wavenumbers. The last part of the spectrum generated by the 852 nm laser is duplicated by the first part of the spectrum generated by the 785 nm spectrum. In addition, the spectrum generated by the 852 nm laser includes spectral peaks not included in the spectrum generated by the 785 nm laser and vice versa. The 852 nm laser corresponds to 11737.1 cm^{-1}, and the 785 nm laser corresponds to 12738.9 cm^{-1}. The Raman spectral shift is calculated by subtracting the absolute wavenumbers from the wavenumber of the laser used to generate the spectrum. The result of doing this is given in the middle plot of Fig. 7. As shown, the duplicated regions of the two spectra now overlap. A single spectrum is generated by scaling the intensities of the overlapping region and then digitally concatenating the spectra at a predetermined tie-point. The result of this is shown in the bottom plot of Fig. 7. As can be observed, the Raman intensities generated by the two lasers are used to construct a single spectrum, which has greater spectral coverage than either spectrum alone. Although it is convenient to scale the spectra using an overlapping region, a significant number of samples may not have peaks in the region of overlap. For this reason, an alternative method of scaling the spectra prior to merger is the ratio of the standard normal variate (SNV). This involves calculating the standard deviations of each laser region after subtracting the region's mean spectral intensity. The ratio of the standard deviation of the 852 region divided

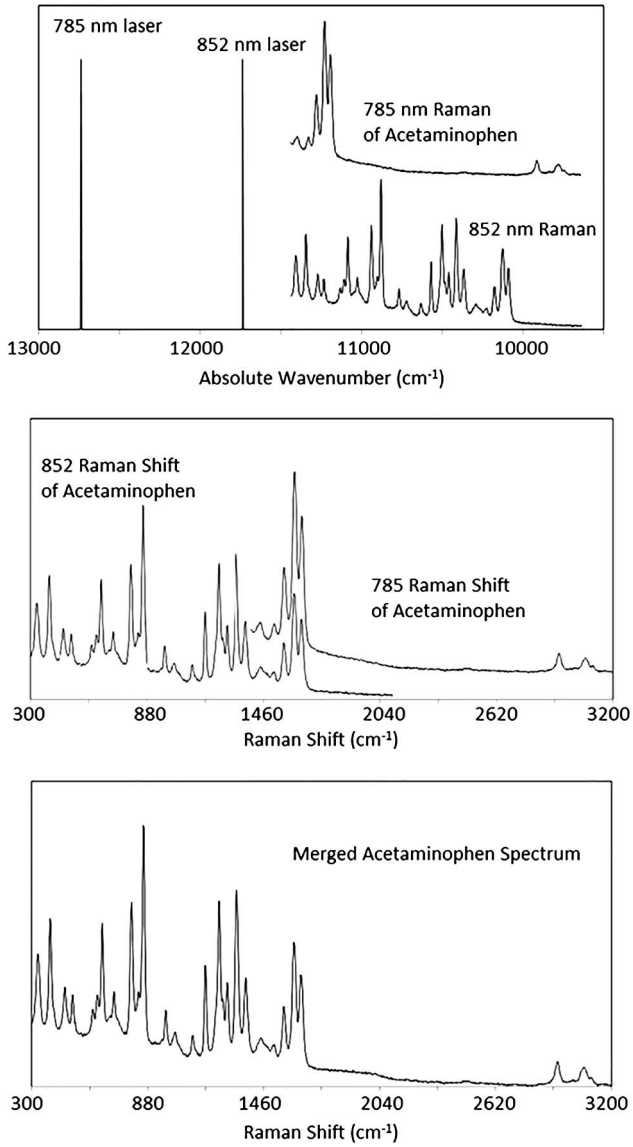

Fig. 7. Processing of the Raman spectra from the dual laser instrument is shown. In the top plot, the Raman spectra generated by the two lasers are plotted on an absolute wavenumber axis with the lasers generating the spectra also indicated with vertical lines. In the middle plot, the spectra are plotted relative to their wavenumber shifts from the lasers generating the spectra. In the bottom plot, the spectra are shown after being merged into a single spectrum.

by the 785 region is then multiplied by the 785 region intensities. This type of scaling (SNV ratio) avoids the requirement of overlapping peaks but is more sensitive to differences in spectral backgrounds between the two Raman. An example of this type of scaling is used in the following example where fluorescent backgrounds have been removed prior to merging the spectra.

7. Application to Fluorescence Removal

Even when using a long excitation wavelength such as 852 nm, fluorescence is still often encountered. For this reason, it is common to use fluorescence-removal

techniques such as shifted excitation Raman difference spectroscopy (SERDS), modulated Raman spectroscopy (MRS), and sequentially shifted excitation Raman spectroscopy (SSE-Raman) [10–18]. In the following example, we show the advantage of the present instrument design over a single-laser design when analyzing a highly fluorescent sample and carrying out SSE-Raman. The design of the single 785 nm instrument has previously been described and uses the same optical configuration as the dual instrument, with the exception of the filters and the laser [10]. A 10 nM solution of 1,1,3,3,3',3'-hexamethyl-indo-tricarbocyanine iodide (Sigma no. 252034) dye was made using acetonitrile as the solvent. The dye was selected because its strong fluorescence is present even in very dilute solutions, and the acetonitrile was selected because it has well-resolved peaks across the entire Raman shift region. The Raman spectrum of the solution was collected using both 785 and 852 nm lasers of the dual-laser instrument as well as using the single-laser 785 nm instrument. The integration time for all spectra was 500 ms.

These spectra are shown in Fig. 8. As can be observed, the fluorescence when exciting with 785 nm lasers is intense while the fluorescence when exciting with 852 nm is weak. Indeed, for the single-laser instrument, the sample had to be slightly defocused to prevent the CCD from saturating. However, for the dual instrument, this was not the case, since only the long wavelength portion of the 785 nm laser spectrum is observed (the high-pass filter removes the shorter wavelength region).

In order to remove the fluorescence from all spectra, seven SSE Raman spectra were acquired for each laser. The spectra acquired for the 852 nm laser are shown in Fig. 9 and were generated by acquiring the spectra at seven laser temperatures starting at

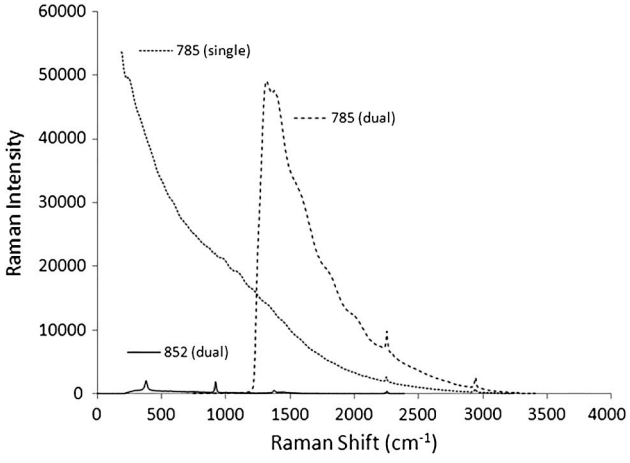

Fig. 8. Raman spectra of a 10 nM solution of 1,1,3,3,3',3'-hexamethylindotricarbocyanine iodide in acetonitrile solvent are shown. The underlying background is due to the fluorescence of the dye while the peaks are due to the Raman of the solvent. The two spectra marked as "dual" were acquired using the dual-laser instrument (serial mode operation), while the spectrum marked as "single" was acquired with the single-laser instrument.

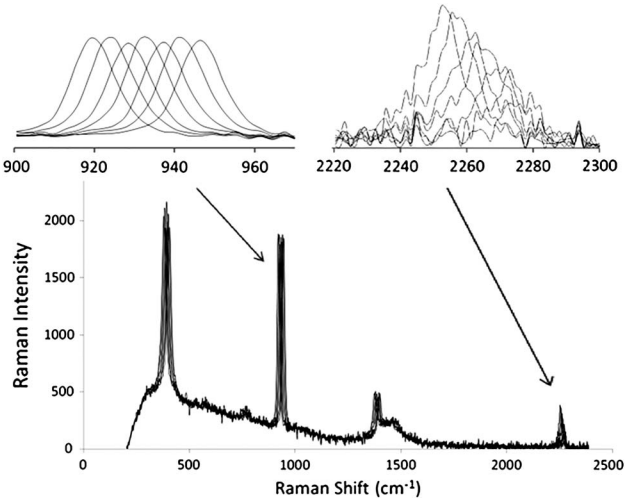

Fig. 9. Raw SSE-Raman spectra of the acetonitrile/dye solution for the 852 nm laser are shown. Only the left-most spectrum corresponds to Raman generated by 852 nm (same spectrum as shown in Fig. 8, 852 dual). The additional six spectra correspond to progressive shifts of the laser of approximately 4 cm^{-1}. Although the Raman shifts with excitation, the underlying fluorescence remains unchanged.

5°C and incrementing by ~5°C six times. An inset in Fig. 9 shows the intense acetonitrile peak at 940 cm^{-1} being sequentially shifted with a temperature-induced excitation shift. As shown, the total shift corresponds to the full width of the Raman band. The SSE Raman spectra were subsequently demodulated using a standard SSE algorithm, which retains the intensities that shift while discarding the intensities, which do not shift [10]. Although the CN stretch at 2250 cm^{-1} is present for the 785 and 852 nm excitation, for the dual-laser experiment, the tie point was set at 2100 cm^{-1}, and the Raman region above 2200 cm^{-1} was discarded for the 852 nm excitation, resulting in no overlapping peaks between the two regions. The CN stretch at 2250 cm^{-1} is shown expanded in the second inset of Fig. 9. For 852 nm excitation, this peak is occurring at a wavelength where the CCD has a low quantum efficiency (1054 nm). As shown in the Fig. 9 inset, with each shift to a longer wavelength, the peak intensity for the CN stretch decreases significantly, which is indicative of the steep and negative slope of the detectors' QE curve. This progressive decrease in intensity along with the resulting low signal-to-noise ratio of this peak makes it difficult to normalize the two spectral regions by normalizing the overlapping peaks. For this reason, the spectral regions for the dual-laser instrument were normalized using the SNV ratio method described above.

For the dual-laser instrument, the two resulting spectra were merged and are shown overlaid with the demodulated spectrum from the single 785 nm instrument in the top plot of Fig. 10. For clarity, the single-laser spectrum is offset by 25,000. Although both instruments are able to successfully remove the fluorescence background, the S/N for

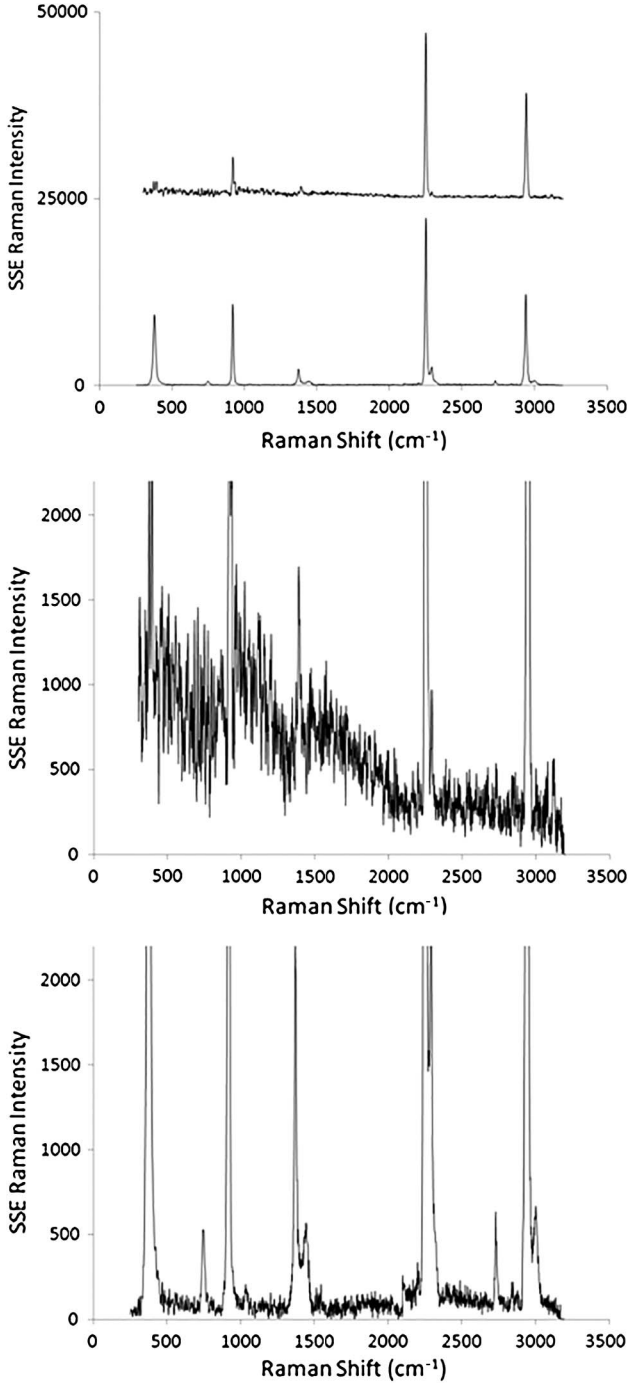

Fig. 10. Top plot shows the demodulated SSE-Raman spectra of the acetonitrile/dye solution for both the single laser (785 nm) instrument and the dual laser (785/852 nm) instrument. The single laser instrument spectrum has been offset by 25,000 counts and is the top spectrum in the top plot. Middle plot shows the expanded baseline region of the single-laser spectrum (no offset), while bottom plot shows the expanded baseline region of the dual laser spectrum.

the dual-laser instrument is significantly higher. This is particularly true for the region of the spectrum, which is generated by the 852 nm laser, where the signal-to-noise is greater by a factor of ~20. However, even in the region where the dual-laser instrument is using the 785 nm laser, the S/N is still significantly higher than the single-laser instrument (~5×). This is due to the fact that a greater laser power density at the sample was used for the dual-laser instrument. This was not possible with the single-laser instrument, since it would have saturated the CCD in the shorter wavelength region, which is required for the single-laser instrument but not for the dual-laser instrument. It is worth noting that since the tie point was 2100 cm^{-1}, the intensity of the 785 nm excitation spectrum for the dual-laser instrument could be increased by a factor of five and still not result in saturation of the CCD (Fig. 8). This would result in an additional 2.24-fold increase in S/N when compared to the single-laser instrument.

Although the 852 nm excitation laser provides the ability to obtain the CN stretching vibration at 2250 cm^{-1}, the use of the 785 nm excitation laser allows a much higher S/N to be obtained for the dual-laser instrument due to the higher quantum efficiency of the CCD. Hence the dual-laser instrument offers additional advantages.

Examination of the baseline in the bottom plot of Fig. 10 reveals the tie point of the spectra at 2100 cm^{-1}. The small inflection in the baseline is a result of using the ratio of SNVs for normalization of the two excitation spectra. The magnitude of the inflection is approximately equal to the magnitude of the baseline noise.

For samples with intense fluorescence, there is a significant advantage using the longer wavelength excitation even when using shifted-excitation fluorescence removal techniques. The 20× improvement is particularly significant when considering the fact that the 852 nm laser should result in only 72% of the 785 nm signal, considering the lower scattering efficiency of the longer wavelength. In addition to the advantages considering fluorescence, the dual-laser instrument also has the advantage of spatial compression. In the present example, this results in the dual-laser instrument requiring only 65% of the CCD dimension corresponding to dispersion (i.e., only 650 vertical pixels are required for the dual instrument while 1024 are required for the single-laser instrument). Although this advantage is not utilized in the current comparison, future designs could take advantage of this feature by either using a smaller CCD length or by increasing the dispersion to realize higher resolution. The use of DBR diode lasers in the present design is also significant, since it allows temperature tuning of both lasers across a broad temperature range without incurring mode hops. We have previously reported on this feature, but with the gaining popularity of complex excitation shifting algorithms, it greatly expedites data collection of complex shifting sequences [19]. It is also a significant advantage to have both lasers mounted on the same TEC, which greatly simplifies simultaneous and rapid temperature tuning. The lock-in time for each temperature used in the current experiments is 200 ms, which is approximately equal to

the time it takes the laser to rise to a stable output when switched on. For the described SSE Raman spectra, the total acquisition time is equal to the integration time (7×500 ms $= 3500$ ms) plus the temperature-tuning time (6×200 ms $= 1200$ ms). This gives a total acquisition time of 4.7 s. Although we have not investigated the impact of highly scattering solids on the spatial resolution of the two CCD images, which result from parallel operation (Fig. 6), it would be expected that such samples may result in overlap of the spectral images and would require selective vertical binning of the CCD pixels to avoid spectral mixing.

8. Conclusion

The use of spatial compression with dual 785 and 852 nm lasers for Raman excitation allows for the maximization of both spectral coverage and fluorescence rejection when compared with the use of either laser by itself. Due to the 2D nature of the CCD and the dual-laser design, it is possible to either carry out both laser measurements simultaneously with identical integration periods (parallel mode) or to carry out each measurement in sequence (serial mode) with separate integrations for each laser.

References

1. X. Li, T. Yang, and S. Li, "Discrimination of serum Raman spectroscopy between normal and colorectal cancer using selected parameters and regression-discriminant analysis," Appl. Opt. **51**, 5038–5043 (2012).
2. J. B. Cooper, "Chemometric analysis of Raman spectroscopic data for process control applications," Chemometrics and Intelligent Laboratory Systems **46**, 231–247 (1999).
3. J. B. Cooper, J. Aust, C. Stellman, K. Chike, M. L. Myrick, R. Schwartz, and M. Longmire, "Raman spectroscopy with a low-cost imaging CCD array," Spectrochim. Acta Part A **50**, 567–575 (1994).
4. B. Chase, "FT-Raman spectroscopy: a catalyst for the Raman explosion?" J. Chem. Education **84**, 75–80 (2007).
5. M. Maiwald, G. Erbert, A. Klehr, H. D. Kronfeldt, H. Schmidt, B. Sumpf, and G. Traenkle, "Rapid shifted excitation Raman difference spectroscopy with a distributed feedback diode laser emitting at 785 nm," Appl. Phys. B **85**, 509–512 (2006).
6. Q. Fan, J. Cao, Y. Liu, B. Yao, and Q. Mao, "Investigations of the fabrication and the surface-enhanced Raman scattering detection applications for tapered fiber probes prepared with the laser-induced chemical deposition method," Appl. Opt. **52**, 6163–6169 (2013).
7. R. H. Brody, E. A. Carter, H. G. M. Edwards, and A. M. Pollard, "FT-Raman spectroscopy, applications," in *Encyclopedia of Spectroscopy and Spectrometry*, L. John, ed., 2nd ed. (Academic, 1999), pp. 732–740.
8. P. Vítek, E. M. A. Ali, H. G. M. Edwards, J. Jehlička, R. Cox, and K. Page, "Evaluation of portable Raman spectrometer with 1064 nm excitation for geological and forensic applications," Spectrochim. Acta Part A **86**, 320–327 (2012).
9. Z. Li, M. J. Deen, Q. Fang, and P. R. Selvaganapathy, "Design of a flat field concave-grating-based micro-Raman spectrometer for environmental applications," Appl. Opt. **51**, 6855–6863 (2012).
10. J. B. Cooper, M. Abdelkader, and K. L. Wise, "Sequentially shifted excitation Raman spectroscopy: novel algorithm and instrumentation for fluorescence-free Raman spectroscopy in spectral space," Appl. Spectrosc. **67**, 973–984 (2013).
11. C. Krafft, S. Dochow, N. Bergner, J. H. Clement, B. B. Praveen, M. Mazilu, R. Marchington, K. Dholakia, and J. Popp, "Raman spectra of single cells with autofluorescence suppression by modulated wavelength excitation," Proc. SPIE **8219**, 82190F (2012).
12. B. Balagopal, P. C. Ashok, R. F. Marchington, M. Mazilu, A. D. Gillies, S. Herrington, A. Riches, and K. Dholakia, "Fluorescence suppression using modulated wavelength Raman spectroscopy for tissue and cell analysis," in *OSA Technical Digest* (Optical Society of America, 2012), paper JM3A.35.
13. E. Canetta, M. Mazilu, A. C. De Luca, A. E. Carruthers, K. Dholakia, S. Neilson, H. Sargeant, T. Briscoe, C. S. Herrington, and A. C. Riches, "Modulated Raman spectroscopy for enhanced identification of bladder tumor cells in urine samples," J. Biomed. Opt. **16**, 037002 (2011).
14. W. Zou, Z. Cai, and J. Wu, "Fluorescence rejection by shifted excitation Raman difference spectroscopy,"Proc. SPIE **7855**, 78551M (2010).
15. M. Mazilu, A. C. De Luca, A. Riches, S. Herrington, and K. Dholakia, "Modulated Raman spectroscopy technique for real-time fluorescence rejection," Proc. SPIE **7568**, 75680M (2010).
16. M. Mazilu, A. C. De Luca, A. Riches, C. S. Herrington, and K. Dholakia, "Optimal algorithm for fluorescence suppression of modulated Raman spectroscopy," Opt. Express **18**, 11382–11395 (2010).
17. M. A. d. S. Martins, D. G. Ribeiro, E. A. Pereira dos Santos, A. A. Martin, A. Fontes, and H. d. S. Martinho, "Shifted-excitation Raman difference spectroscopy for in vitro and in vivo biological samples analysis," Biomed. Opt. Express **1**, 617–626 (2010).
18. J. Cooper, M. F. Abdelkader, and K. Wise, "Method and apparatus for acquiring Raman spectra without background interferences," U.S. Patent, 8,570,507 B1 (29 October 2013).
19. J. B. Cooper, P. E. Flecher, S. Albin, T. M. Vess, and W. T. Welch, "Elimination of mode hopping and frequency hysteresis in diode laser Raman spectroscopy: the advantages of a distributed Bragg reflector diode laser for Raman excitation," Appl. Spectrosc. **49**, 1692–1698 (1995).